Carbohydrate Polymers 135 (2016) 215–224

Contents lists available at ScienceDirect

Carbohydrate Polymers

journal homepage: www.elsevier.com/locate/carbpol

A uniaxially oriented nanofibrous cellulose scaffold from pellicles produced by *Gluconacetobacter xylinus* in dissolved oxygen culture

Aya Nagashima, Tsubasa Tsuji, Tetsuo Kondo*

Graduate School of Bioresource and Bioenvironmental Sciences, Kyushu University, 6-10-1 Hakozaki, Higashi-ku, Fukuoka 812-8581, Japan

ARTICLE INFO

Article history:
Received 7 July 2015
Received in revised form 22 August 2015
Accepted 26 August 2015
Available online 2 September 2015

Keywords:
Culture using dissolved oxygen
Gluconacetobacter xylinus
Stretchable nanocellulose pellicle
Nano-orientation
Nanofibrous film

ABSTRACT

An aerobic, Gram-negative bacterium, *Gluconacetobacter xylinus*, was successfully employed to produce a stretchable cellulose nanofiber pellicle using dissolved oxygen in a conventional cultured medium. The obtained nanofibers were highly crystalline with the metastable cellulose I_α phase being apparently the dominant phase by more than 90%. The obtained pellicle could be stretched by up to 1.5 times to provide oriented crystalline nanofibrous films. Low heating of the nanofibrous film induced the transformation of the dominant cellulose I_α crystalline phase into the I_β crystalline phase without a loss of crystallinity or the high Young's modulus. The film also exhibited unique and anisotropic viscoelastic and mechanical properties as well as superior thermal stability compared with conventional high-performance synthetic polymeric materials. In addition, when *G. xylinus* cells were transferred to the oriented surface after stretched, they started to synthesize cellulose ribbons that parallel the nanofiber orientation of the substrate. This function as a template was evidenced by direct video imaging of the motion of the bacteria. The application of a bacterial culture using dissolved oxygen in the medium offers the fabrication of novel anisotropic and nanofibrous scaffold of cellulose I_α.

1. Introduction

In culture medium, *Gluconacetobacter xylinus* (formerly *Acetobacter xylinum*) secretes ribbon-like cellulose nanofibers of ca. 50 nm in width and 10 nm in thickness. The cellulose nanofibers undergo random movements of the bacterium during fiber secretion to form three dimensional networks that result in gel-like membranes called pellicles at the air/water interface. These pellicles have been extensively studied as they are promising biobased materials with versatile properties, e.g. biocompatibility (Helenius et al., 2006), high water absorption capacity, high crystallinity, and high mechanical strength (Yamanaka, Watanabe, & Kitamura, 1989). Further investigations have been carried out to open up the application of such pellicles to other fields, including tissue engineering (Bäckdahl, Esguerra, Delbro, Risberg, & Gatenholm, 2008; Bodin, Concaro, Brittberg, & Gatenholm, 2007), electronic devices (Shah & Brown, 2005), emulsifiers (Blaker, Lee, Li, Menner, & Bismarck, 2009), and nanocomposites (Yano et al., 2005). Most of the above applications rely on the unique three-dimensional "nanocellulose" network structure of the pellicle, as a key for their function. The author has extensively studied their unique alignment process of microbial cellulose nanofibers on the scaffolds (Kondo & Kasai, 2014; Kondo et al., 2002, 2012) and also proposed preparation of the microbial single nanofibers (Kose & Kondo, 2013; Kose, Kasai, & Kondo, 2011; Kose, Mitani, Kasai, & Kondo, 2011) to probe further applications.

When *G. xylinus* is in the presence of D-glucose in the culture medium (Hestrin & Schramm, 1954), two reactions proceed that result in either cellulose or adenosine triphosphate (ATP) (Ross, Mayer, & Benziman, 1991), as shown in Fig. 1. In both pathways, D-glucose is initially converted into glucose-6-phosphate (Glc-6-P) by glucokinase (Benziman & Rivetz, 1972). In the case of synthesizing cellulose, Glc-6-P is first transferred into uridine diphosphate glucose (UDP-Glc), which is a precursor of polymerization (Swissa, Aloni, Weinhouse, & Benizman, 1980). Cellulose is then synthesized from UDP-Glc by cellulose synthesizing enzymes (CesA) in terminal complexes (TCs) located on the outer membrane of the bacterial body (Kimura, Chen, Saxena, Brown, & Itoh, 2001).

In the case of producing ATP, Glc-6-P ultimately produces CO_2 and H_2O after following the pentose phosphate (PP) pathway, the tricarboxylic acid (TCA) cycle, and undergoing electron transfer to produce ATP. In an alternative pathway, D-glucose is first converted into gluconate-6-phosphate (gluconate-6-P) via gluconate without passing Glc-6-P, and then proceeds via the PP pathway. It is noted that gluconate-6-P also converts into Glc-6-P via fructose-6-phosphate (Fru-6-P) through the PP pathway and

* Corresponding author.
E-mail address: tekondo@agr.kyushu-u.ac.jp (T. Kondo).

http://dx.doi.org/10.1016/j.carbpol.2015.08.077
0144-8617/

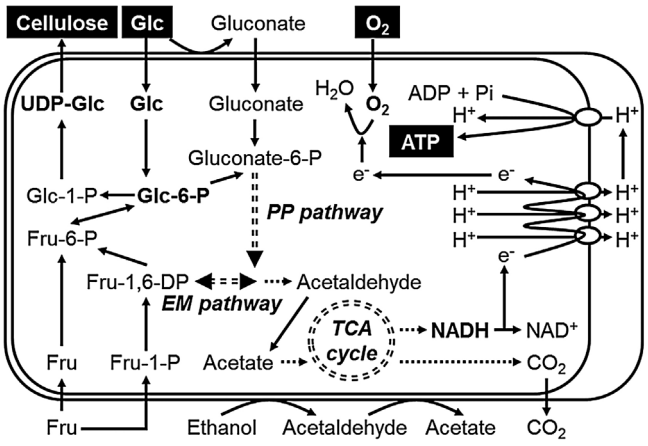

Fig. 1. A proposed pathway of glucose metabolism in *G. xylinus* (Benziman & Rivetz, 1972; Hestrin & Schramm, 1954; Kose & Kondo, 2013; Ross et al., 1991). The abbreviations used are as follows: Glc: glucose, Fru: fructose, PP: pentose phosphate, EM: Embden–Meyerhof, and TCA: tricarboxylic acid.

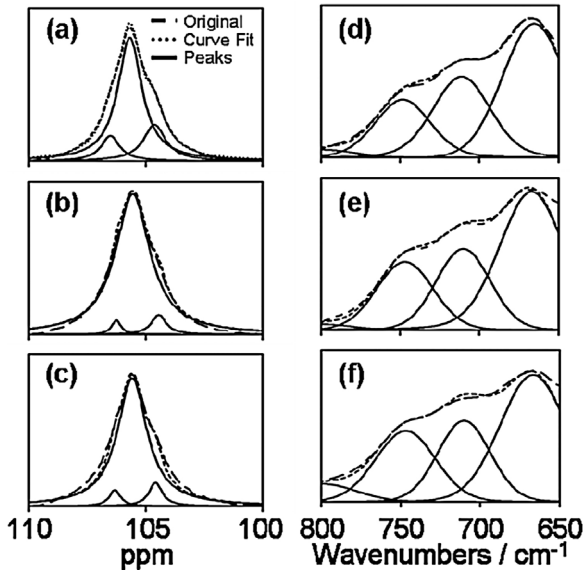

Fig. 2. CP/MAS ^{13}C NMR (a–c) and corresponding FTIR (d–f) spectra of the gel-like cellulose pellicle formed in the culture medium: (a, d) culture medium only, (b, e) culture medium covered with silicone oil, and (c, f) culture medium covered with silicone oil after bubbling N_2 through the culture medium.

the Embden–Meyerhof (EM) pathway. During the above energy metabolism, *G. xylinus* requires an aerobic atmosphere, because any oxygen that is introduced into a bacterial body acts as an electron acceptor in the electron transfer system. If no oxygen is available for use by *G. xylinus*, the nicotinamide adenine dinucleotide (NADH) in the system is assumed to be present in a reduced form. It is thus incapable of receiving electrons (not shown in Fig. 1), resulting in an inability to produce ATP, thereby inducing an increase in the consumption of D-glucose for synthesizing cellulose. Namely, an oxygen atmosphere may be an important factor in determining the consumption of D-glucose for either synthesizing cellulose or producing ATP. To date, there have only been a few reports that have focused on increasing the cellulose production yield by modulating the concentration of gaseous oxygen or dissolving oxygen in the culture media (Bae & Shoda, 2005; Chao, Sugano, & Shoda, 2001; Cheng, Wang, Chen, & Wu, 2002; Hwang, Yang, Hwang, Pyun, & Kim, 1999; Naritomi et al., 2002; Setyawati, Chien, & Lee, 2007; Vandamme, Baets, Vandaelen, Joris, & Wulf, 1998; Watanabe & Yamanaka, 1995). However, none of these reports have investigated in detail whether *G. xylinus* can synthesize cellulose using only dissolved oxygen in the culture medium, instead of gaseous oxygen from the atmosphere.

In this article, we attempted to incubate *G. xylinus* in an oxygen-lacking, stressed environment to determine if the bacterium could synthesize cellulose using the dissolved oxygen in the culture medium. As a result, *G. xylinus* successfully secreted cellulose nanofibers rich in the I_α crystalline phase for subsequent use in formation of a unique pellicle, which can be stretched, exhibiting advanced properties as described below.

2. Experimental

2.1. Materials

Components of the Schramm–Hestrin (SH) culture medium (Hestrin & Schramm, 1954) were: D-glucose, citric acid and sodium hydroxide of culture grade, which were purchased from Wako Pure Chemical Industries Ltd., Osaka, Japan; disodium hydrogen phosphate heptahydrate of culture grade was purchased from Nacalai Tesque, Shiga, Japan; and yeast extracts and peptone were provided by Becton, Dickinson and Company, New Jersey, USA.

2.2. Bacterial culture using dissolved oxygen in a culture medium

G. xylinus (NQ-5: ATCC53582) was inoculated into a culture medium in a sterilized cylindrical test tube, and statically cultured at 30 °C for 2 weeks to produce a normal culture. The SH culture medium was covered with silicone oil (KF96 100 CS, Shin-Etsu Chemical Co. Ltd., Tokyo, Japan) to prevent the *G. xylinus* inoculated in the culture medium from being exposed to oxygen gas in the atmosphere. To set up a further oxygen-lacking environment, the culture medium was bubbled with nitrogen gas under a diminished pressure, prior to covering with the silicone oil. After 2 weeks' incubation, a gel-like pellicle was formed at the interface between the culture medium and the silicone oil (see Fig. 2b and c), similar to the pellicle formed in normal culture (Fig. 2a). The obtained material was collected and washed with 0.1% aqueous NaOH solution at 80 °C for 4 h, and then successively washed with water over 3 days to remove protein, bacterial cells, and other residues. After, the purified material was dried at 130 °C for 24 h (Tomita, Tsuji, & Kondo, 2009) and then weighed. For viscoelastic measurements, the sample was freeze-dried and subsequently fixed to a sample holder. During the incubation, the dissolved oxygen level in the culture medium was measured every second day using a dissolved oxygen analyzer (OM-51, Horiba, Ltd., Kyoto, Japan).

2.3. Preparation of an oriented nanofibrous film

The gel-like pellicle obtained in the bacterial culture was uniaxially drawn using a purpose-made manual stretching device as follows: the sample was cut into strips of approximately 30 mm length and 10 mm width. The specimens were then clamped in the stretching device and elongated uniaxially at room temperature. The drawing process was performed while the sample was kept wet. Following air-drying of the stretched specimen with a fixed state, it was dried at 130 °C for 24 h to completely remove any free and absorbed water. Non-stretched samples were prepared as references under the same drying procedure with a fixed state in the device to prevent shrinking. For the viscoelastic measurements, the same sample drying process was employed.

2.4. Measurements

Prior to the following measurements, the sample specimens were rapidly-frozen with liquid nitrogen to be provided for vacuum freeze-drying.

Fourier transform infrared spectroscopy (FTIR). FTIR spectra for the dried film samples were obtained using a FTIR-620 spectrophotometer (Jasco, Inc., Tokyo, Japan) equipped with a TGS detector. Thirty-two FTIR spectra were collected at 2 cm^{-1} resolution in the 4000 to 400 cm^{-1} wavenumber region. To determine the % crystalline fraction of the I_α crystalline phase in the whole cellulose crystalline phase, the characteristic IR absorption bands (Sugiyama, Persson, & Chanzy, 1991) at 750 cm^{-1} for I_α and at 710 cm^{-1} for I_β were deconvoluted by using a Gaussian–Lorentzian curve fitting analysis until R^2 is over 99.9% (Kondo, 1997). The IR index for the I_α fraction (f_{IR}) was calculated based on the band areas for I_α (A_{750}) and I_β (A_{710}), as $f_{IR} = A_{750}/(A_{750} + A_{710})$ (Yamamoto, Horii, & Hirai, 1996). The corresponding I_α fraction was obtained using our own equation described in the following section, which was determined by the relationship between the I_α fraction in the IR spectra and the data obtained from solid state CP/MAS ^{13}C NMR measurements (f_{NMR}) (Yamamoto et al., 1996).

Cross-polarization/magic angle spinning (CP/MAS) ^{13}C NMR measurements. The CP/MAS ^{13}C NMR measurements of the same sample specimens for the FTIR described above were performed using a Chemagnetics CMX 300 spectrometer (Chemagnetics, USA) operating at 75.5 MHz with a 4 mm MAS double resonance probe and ZrO_2 rotors. The sample spinning frequency was 10 kHz, the repetition time was 3 s and the cross-polarization (CP) contact time was 1 ms. To determine the I_α fraction in the whole cellulose crystalline phase, the characteristic ^{13}C NMR signals due to the C_1 carbons were deconvoluted by a Lorenzian curve fitting analysis (Kataoka & Kondo, 1999; Yamamoto & Horii, 1993). The resulting signal contained both one signal assigned to the I_α crystal lattice and two signals assigned to the I_β crystal lattice. The I_α fraction was calculated according to the following equation:

$$\frac{I_\alpha \text{ fraction}}{\%(f_{NMR})} = \frac{\text{signal areas assigned to } I_\alpha \text{ crystalline phase}}{\text{total areas corresponding to } I_\alpha \text{ and } I_\beta \text{ phases}} \times 100$$

The equation showing the relationship between f_{IR} and f_{NMR} was obtained as:

$$f_{NMR} = 2.23 \times f_{IR} - 0.19.$$

Scanning electron microscopy (SEM). All samples after rapidly freeze-dried described above were coated with gold using an ion sputterer (JFC-1100, JEOL Ltd., Tokyo, Japan) to achieve optimal imaging results. SEM (JSM5600LV, JEOL Ltd., Tokyo, Japan) images were acquired at the accelerating voltage of 15 kV. The gel-like materials were dehydrated using a series of aqueous ethanol solutions: 30, 50, 70, 80, 90, and 100%, and eventually exchanged with 2-methyl-2-propanol, and dried prior to gold coating.

Transmission electron microscopy (TEM). The sample was cut and homogenized at 2.0×10^4 rpm for 5 min using a homogenizer (Physcotoron NS-51: Microtec Co. Ltd., Chiba, Japan) with ultrapure water, resulting in dispersed small pieces of cellulose nanofiber pellicles in water (Kose et al., 2011b). The aqueous dispersion was mounted on copper grids, air dried, and stained negatively with a few drops of 2% uranium acetate/water solution prior to TEM observation (JEM-1010 JEOL, Tokyo, Japan) at the accelerating voltage of 80 kV. The negative films of the acquired images were scanned, digitized, and then the width of a single cellulose nanofiber was measured using Scion Image software (Scion Corp., USA).

Orientation of nanofibers. The degree (D) of orientation of the nanofibers was approximately calculated according to the following equation using the collected SEM images of the individual fibers:

$$D = \frac{180 - \theta^\circ}{180}$$

where θ is the half width of the deviation degree relative to the stretching direction. Nanofibers without stretching effects in the SEM images were neglected.

Crystallinity and orientation of crystalline domains using wide angle X-ray diffraction (WAXD). The crystallinity was calculated according to the following expression:

$$\text{crystallinity}/\% = \frac{\text{total areas of typical crystalline diffraction peaks}}{\text{total areas of crystalline and amorphous peaks}} \times 100$$

To estimate the molecular orientation of the nanofibers in the crystalline domains along the stretching direction, WAXD was employed using nickel-filtered CuK_α radiation produced by a RINT-2500HF X-Ray generator (Rigaku Mechatronics Co. Ltd., Tokyo, Japan) with a 1-mm-diameter pinhole collimator at 40 kV and 200 mA. WAXD intensity curves of the sample films were measured by a transmission method using a scintillation counter with a scanning rate of 0.5°/min. The angular range of the WAXD curves for the equatorial scan to the stretching direction were $2\theta = 5^\circ$–35°. The orientation parameter of crystallites, π, for the stretched films was estimated using the following equation (Togawa & Kondo, 1999).

$$\pi = \frac{180 - H^\circ}{180}$$

where H is the half-width of the azimuthal intensity distribution for the meridional reflection at the (0 0 4) plane.

Total molecular orientation using polarized FTIR. Polarized FTIR was employed to evaluate the total molecular orientation in the oriented nanofibrous films. Thirty-two polarized FTIR spectra were obtained with 2 cm^{-1} resolution in the 4000 to 400 cm^{-1} wavenumber region. The orientation behavior of the main chains was estimated from the dichroic ratios obtained at 1162 cm^{-1} because of the C–O–C asymmetric stretching vibration (Hishikawa, Togawa, & Kondo, 2010). The ratios (R) were calculated in the same manner as reported by Zbinden (Zbinden, 1964):

$$R = \frac{A_\perp}{A_{//}} \quad (0.0 < R < \infty)$$

where $A_\perp$ is the absorbance obtained using radiation polarized perpendicularly to the stretching direction, and $A_{//}$ is the absorbance obtained using radiation polarized parallel to the stretching direction.

Mechanical properties for film samples. To evaluate the crosslinking population density of the cellulose nanofibers in the obtained pellicle, the pellicle was compressed using a rheometer (ARES, Rheometric Scientific, Inc., New Jersey, USA) to remove free water before dynamic viscoelastic measurements. The relative crosslinking population density among the samples was calculated based on the saturated E' values with elevating temperature using the following equation derived from the theoretical equation of rubbery elasticity (Nielsen & Landel, 1994):

$$n = \frac{E'}{3kN_AT}$$

where n is the apparent crosslinking population density, k is Boltzmann's constant, N_A is Avogadro's constant, and T is the temperature of the flat region for E'.

The change in E' of the film samples under a fixed frequency of 10 Hz was also measured as a function of temperature using a

dynamic viscoelastic measuring instrument equipped with an environmental control system (DVA-200, IT Keisoku Co. Ltd., Osaka, Japan). The heating rate was 5 °C per minute from room temperature to 300 °C. The pellicles were freeze-dried and heated in a dry oven at each selected temperature for 24 h before taking measurements as described previously. Then, to examine the influence of water vapor, the measurements were performed under various relative humidity values (10, 30, 50, 70, and 90%). Soon after the measurements, the samples were also subjected to both mechanical strength and contact angle measurements.

The mechanical strength of the film samples was measured using a tension tester (Strograph E-S, Toyo Seiki Seisaku-sho Ltd., Tokyo, Japan). The samples studied were 5 mm in width and 15 mm in length. The measurements were performed at 5 mm/min of the tension rate. The Young's moduli were calculated from the obtained stress–strain curves.

For contact angle measurements, a Drop Master DM-300 (Kyowa Interface Science Co. Ltd., Saitama, Japan) was used. A drop of 1 μL ultrapure water was placed on the surface of the stretched films in an ambient atmosphere of 25 °C and 60% of relative humidity and kept there for 1 s prior to the contact angle measurement.

The surface of the stretched films was observed using a NanoScope IIIa atomic force microscope (AFM, Veeco Instruments, Inc., New York, USA) operated in tapping mode with a J-type piezoelectric scanner and Tap300 metrology probes (single-crystal silicon cantilevers; length: 125 μm, curvature radius: 5–10 nm, spring constant: 40 N m^{-1}, resonance frequency: 200–400 kHz, Veeco Instruments, Inc.). AFM observations were performed in air at room temperature and carried out at five different regions (scan size: 5 μm × 5 μm) across the surface of each sample. The morphological data of the images were analyzed using the AFM-accessory software (Nanoscope version 5.12b36).

3. Results and discussion

3.1. Characterization of gel-like pellicles secreted under an oxygen-lacking environment

In a normal (uncovered) culture medium as a reference, *G. xylinus* secreted cellulose nanofibers to form a pellicle at the interface between the culture medium and air. When the bacteria were cultured in a medium covered with silicone oil, a gel-like pellicle still formed at the interface between the culture medium and the silicone oil (see supporting data Figure 1b and c). This indicates that *G. xylinus* could secrete cellulose nanofibers presumably using oxygen that was dissolved in the culture medium. Therefore, changes in the amounts of dissolved oxygen in the culture medium were monitored during the bacterial culture. When the bacterium was not inoculated in the culture medium, the amount of dissolved oxygen in the culture medium was maintained without any significant change, irrespective of whether it was covered with silicone oil or not. On the other hand, the amount of dissolved oxygen in the culture medium was drastically decreased when inoculated with the bacterium, and then reached to maintain at a certain low value less than 2 mg L^{-1} for all the systems (see supporting data Figure 1d and e).

In a separate study, culture medium covered with silicone oil was first purged with nitrogen gas to remove any dissolved oxygen from the culture medium. After purging, subsequent measurements of the oxygen level in the culture medium showed an increase in the amount of dissolved oxygen, suggesting that gaseous oxygen permeates from the ambient atmosphere through the silicone oil to dissolve into the culture medium (as represented by the open triangles in supporting data Figure 1d and e). It was likely to that the atmospheric oxygen were gradually penetrating and dissolving into the culture medium to recover to a certain level of the dissolved amount. The changing behavior of the dissolved oxygen in the culture medium before and after inoculation with *G. xylinus* indicated that the *G. xylinus* bacterium survived at least in the dissolved oxygen in the culture medium, although the decrease in dissolved oxygen was not simply due to only the bacterial consumption. In the culture medium covered with silicone oil, *G. xylinus* used the dissolved oxygen in the culture medium and any gaseous oxygen present in the ambient atmosphere to stay alive.

The pH values in the uncovered and covered culture media fell to acidic values of 4 and 5 (data not shown), respectively. This indicates that the bacterium can still produce acetic acid irrespective of whether the dissolved oxygen in the culture medium is used. The observed difference between the two pH values might be caused as a result of the smaller volume of ATP produced by the bacterium in the oxygen-lacking environment (see Fig. 1). *G. xylinus* with a low yield of ATP to result in having a lower activity appeared to grow slower in this anaerobic conditions, and thus one could easily assume the lower population in this culture because of the lower density of crosslinking of bacterial nanofibers, although the bacterial populations were not correctly measured. It should be also referred that as atmospheric O_2 was permeable through the silicone oil layer, this would be a most probable cause for the observed changes in pH.

Fig. 2 shows the CP/MAS ^{13}C NMR spectra (a–c) of the gel-like cellulose pellicle in the 110–100 ppm range and the FTIR spectra (d–f) in the 800–650 cm^{-1} range. The CP/MAS ^{13}C NMR and FTIR measurements confirm that all the nanofibrous films consist of cellulose I nanofibers (Atalla & VanderHart, 1984; Marrinan & Mann, 1956; VanderHart & Atalla, 1984), supporting the observation that *G. xylinus* can synthesize cellulose nanofibers even using oxygen dissolved in the culture medium. It should be noted that the cellulose pellicle produced under an oxygen-lacking environment is rich (90%) in the metastable cellulose I_α fraction, which was much higher when compared with the 70% value from the nanofibers secreted in the control culture. The physical properties are listed in Table 1.

To understand why the cellulose I_α crystalline phase is richer in the oxygen-lacking environment, we hypothesize that the rate of synthesizing cellulose increases as a result of stress–response behavior, and that the stronger secretion induced by the increasing rate results in the formation of the metastable cellulose I_α crystalline phase (Horii, Yamamoto, Kitamaru, Tanahashi, & Higuchi, 1987; Kataoka & Kondo, 1996, 1998; Sugiyama, Okano, Yamamoto, & Horii, 1990; Sugiyama et al., 1991; Yamamoto & Horii, 1994). The increase in the I_α fraction implies, to some extent, that stress induced during the crystallization phase, results in the formation of the metastable triclinic I_α crystalline phase. An oxygen-lacking environment might preferentially induce the consumption of D-glucose for synthesizing cellulose. Then, the rate of synthesizing cellulose may increase during the initial stage, causing more stress to be exerted than usual. This can contribute, more or less, to the nascent cellulose being crystallized in the meta-stable triclinic I_α crystalline phase. Further investigation is required for determining the initial rate during the cellulose nanofiber secretion. The obtained microbial cellulose (MC) pellicle having a richer cellulose I_α crystalline phase is most probably biocompatible and can be used in a variety of medicinal applications (Bodin et al., 2007; Bäckdahl et al., 2008).

The cellulose pellicle produced using a normal culture as the reference was made up of cellulose nanofibers, as shown in Fig. 3a. The cellulose pellicles formed in culture media covered with silicone oil also formed nanofibrous network structures, as shown in Fig. 3b and c. This shows that *G. xylinus* produces cellulose nanofiber networks even in a sealed environment void of any atmospheric oxygen, and that it relies on the dissolved oxygen in the culture

Table 1
The fraction of cellulose I_α crystalline phase determined by CP/MAS ^{13}C NMR spectra, together with other related physical values of the MC pellicle formed in each culture medium.

MC pellicle	a^*	b^*	c^*
I_α fraction (%)	70	92	88
Relative dry weight (%)	100	9	11
Crosslinking density (10^{-1} mol cm^{-3})	4.80 ± 0.76	3.17 ± 1.17	3.07 ± 0.26
Fiber width (nm)	67 ± 24	47 ± 16	45 ± 14

* MC pellicle formed in the culture medium: (a) non-covered, (b) covered with silicone oil and (c) covered with silicone oil after N_2 babbling.

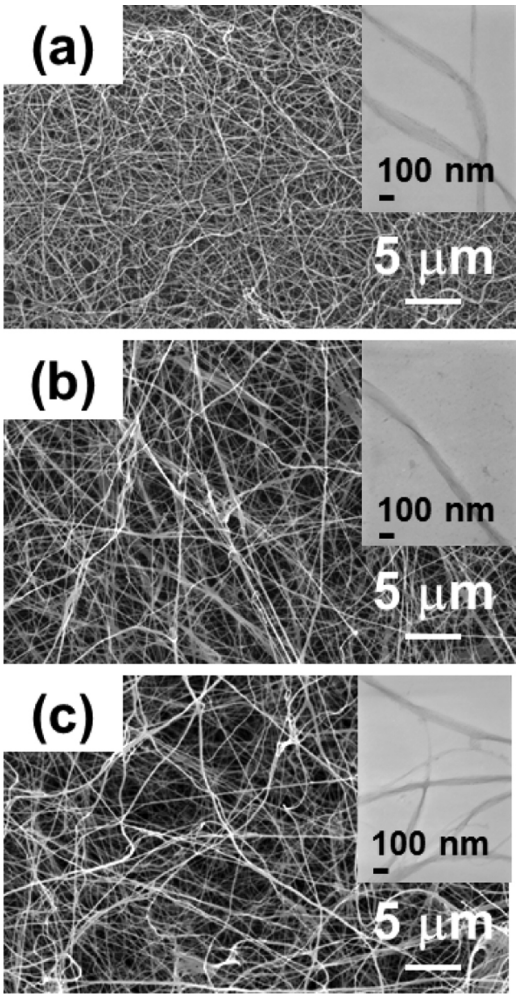

Fig. 3. Scanning electron microscopic (SEM) images of the cellulose pellicle formed in the culture medium: (a) culture medium only, (b) culture medium covered with silicone oil, and (c) culture medium covered with silicone oil after bubbling N_2 through the culture medium. The insets indicate the transmission electron microscopic (TEM) images of the single cellulose nanofibers produced in the individual culture medium.

medium. However, when compared with the control sample, the nanofibers used to form the pellicles in the culture medium covered with silicone oil appeared to be less densely populated and thinner (see the corresponding figures). The single cellulose nanofibers produced in the oxygen-lacking environment exhibit widths of less than two thirds (ca. 45 nm) that of the widths of normal nanofibers, as shown in the TEM image (see inset in Fig. 3).

Table 1 lists the relative dry weights and crosslinking population densities of the nanofibers for each pellicle. The relative dry weight of the pellicle in this study corresponded to about one-tenth of the control sample. This may be because a sufficient amount of ATP required for the synthesis might not be generated using the dissolved oxygen in the culture medium, thereby causing the bacterial activity to be unstable. The apparent crosslinking population density of the nanofibers was lower than that of the control sample, as supported by the corresponding SEM images (see Fig. 3b and c). Namely, fewer and thinner nanofibers were secreted by *G. xylinus* using the dissolved oxygen in the culture medium, resulting in the formation of fewer crosslinkages. These results indicated that the oxygen-lacking environment might reduce the activity of the terminal complexes (TCs) located on the outer membrane of the bacterial body, which are aggregates of cellulose synthesizing enzymes designed to secrete the sub-elementary fibrils.

3.2. Orientation and induced physical properties of the stretched films

To date, the cellulose pellicles produced by *G. xylinus* under the SH culture media have been incapable of being stretched because of the high crosslinking population density of the nanofibers. The nanocellulose pellicles obtained in an oxygen-lacking environment could be uniaxially stretched because of the fewer and thinner nanofibrous crosslinkages. In practice, the nanocellulose pellicles could be uniaxially stretched by up to 1.5 times using a purpose-made stretching device. The scanning electron microscopy (SEM) image (Fig. 4b) of the stretched cellulose pellicle as a fibrous film is compared with the initial film (Fig. 4a) prior to stretching. As a result of the uniaxial stretching, the random fiber-arrangement was well-oriented along the stretching direction, although some non-oriented fibers still remained. The value of *D*, the apparent degree of orientation of the nanofibers, reached over 90% statistically (in the limited more than 50 areas stretched) based on the fiber-aligned SEM image.

The WAXD images of the corresponding samples exhibited a slight change in the diffraction pattern of the very thin nanofibrous film when compared before (c) and after (d) stretching (Bohn, Fink, Ganster, & Pinnow, 2000). The diffraction pattern (d) of the nanofibrous film after stretching still showed a broad arc, indicating the formation of fairly disordered crystalline domains in the fibrous film. The value of π as the degree of orientation of the crystalline domains, which is a lower hierarchical level than the nanofiber level, was calculated to be 74%. The disarray of nanofiber affects the order of the crystalline domains more than the hierarchical level of the crystalline domains. This detailed information, together with supporting data based on the AFM image (see Fig. 4f), indicates that although there was a high tendency of nanofiber orientation, the direction was not perfectly uniaxial. Presumably, a small angle X-ray diffraction study of the same sample, which could reveal the larger scaled orientation, would correspond well to the SEM image results. In addition, both WAXD diffraction profiles exhibited three typical diffraction peaks assigned to the native cellulose crystalline lattice. The degree of crystallinity of the stretched nanofibrous film was calculated to be 86%, which is almost identical to that for the non-stretched samples.

The polarized FTIR spectra obtained for the stretched film imply the further lower scale than the order of crystalline domains; namely, a molecular orientation level. In the absorption band at 1162 cm^{-1} because of C–O–C asymmetric stretching of the

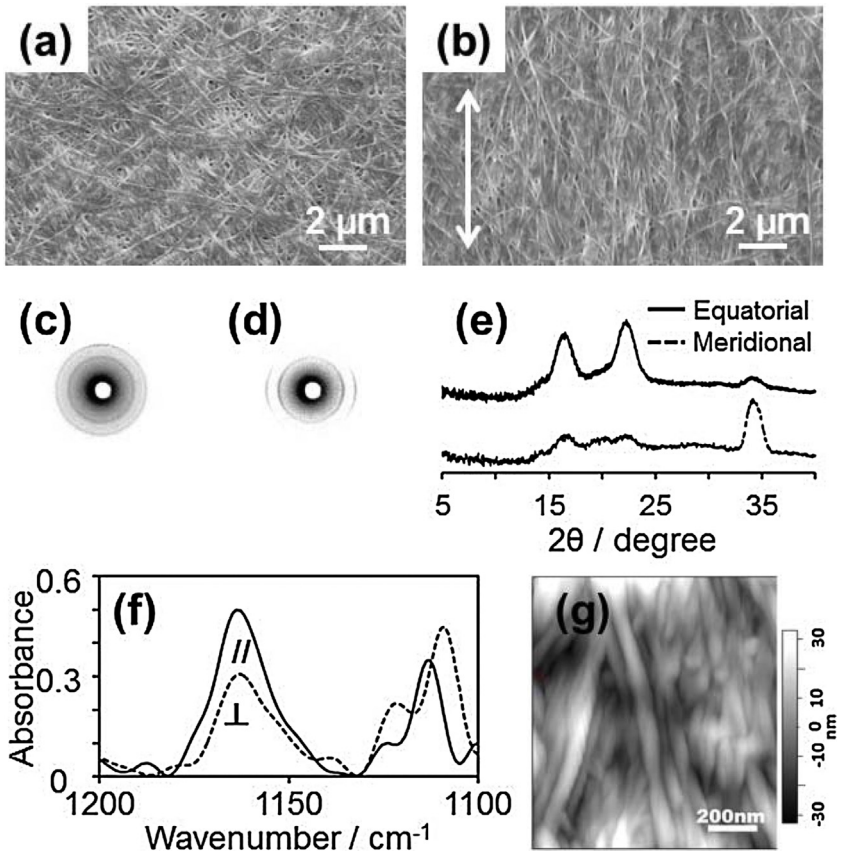

Fig. 4. Scanning electron microscopic (SEM) images (a, b) and WAXD images (c, d) of the cellulose pellicle sample (a, c) and nanofibrous films stretched by up to 1.5 times (b, d). The white arrow in (b) indicates the stretching direction. (e) WAXD intensity curves in equatorial and meridional directions for nanofibrous films stretched by up to 1.5 times (b, d). (f) The bridge C–O–C stretching band (1162 cm^{-1}) in the polarized infrared spectra for the stretched film; the upper line (//) represents the electric vector parallel to the stretching direction and the bottom line (⊥) represents the electric vector perpendicular to the stretching direction. (g) AFM surface image of the stretched cellulose pellicle. Scale bar indicates 200 nm.

glucosidic linkage, the absorbance produced by the radiation polarized parallel to the stretching direction ($A_{//}$) was higher than that for the absorbance produced by the radiation polarized perpendicular to the stretching direction ($A_{\perp}$) (see Fig. 4e). The intensity ratio, R, of the above peaks, was calculated to be 0.62. This value indicates that the uniaxial stretching of the cellulose pellicle by up to 1.5 times enhanced the orientation of the main chains toward the stretching direction. However, the degree of orientation at this scale was also lower than that of the nanofibers based on the SEM observation. The disarrangement of nanofibers in the stretched pellicle is also likely to attribute to this inconsistency.

3.3. Physical properties of stretched nanofibrous films

The storage moduli, E', values of the cellulose nanofibrous films before and after stretching maintained a constant value of ca. 3.0 GPa with elevating temperature under a fixed frequency, as shown in Fig. 5a. The E' value of the film samples indicated the superior thermal stability of the cellulose nanofibrous films, regardless of the fiber orientation. The negligible difference in the E' values between the unstretched and stretched films indicated that the E' value strongly depends on the initial population of crosslinkages of the nanofibers. In addition, the E' value obtained for the cellulose nanofibrous films after stretching exhibited a significant change more remarkably in the tan δ curve at 230 °C.

A marked difference was discovered in the change in % crystalline fraction of allomorphs of the cellulose nanofibers with increasing atmospheric temperature. Fig. 5b shows the changes of the I_α crystalline fraction in the cellulose nanofibers obtained in this study with elevating temperature. The % crystalline fraction of cellulose I_α in the cellulose nanofibers rapidly decreased from 90% to 75% as the temperature was increased from room temperature to over 80 °C. The % crystalline fraction of the cellulose I_α crystalline phase in the cellulose nanofibers for the normal cellulose pellicle was maintained at ca. 75% in the same temperature range. This may be because of the thinner cellulose nanofibers obtained in this study, which are more readily susceptible to changes in thermal conductivity, and/or changes in morphology, including crystalline allomorphs.

Interestingly, it was observed that a decrease in the crystalline % fraction of the I_α crystalline phase in the cellulose nanofibers obtained in this study hardly occurred in the temperature range from 80 °C until 150 °C. At temperatures over 150 °C, the crystalline % fraction of the I_α crystalline phase in the sample exhibited a similar decreasing behavior to that in the normal cultured sample. Then, a further marked decrease in the I_α crystalline phase occurred at 230 °C, corresponding to the change in tan δ at 230 °C. On the other hand, the change in the crystalline % fraction of the cellulose I_β crystalline phase in the cellulose nanofibers obtained in this study corresponded in an opposite manner to that of the I_α crystalline fraction; namely, an increase from ca. 10% to 40% occurred with elevating temperature from 25 °C to 230 °C. Eventually, the crystalline % fraction of the I_β crystalline phase in the cellulose nanofibers obtained in this study superseded the crystalline % fraction of the I_α crystalline phase. During the crystalline transformation, the total crystallinity in the nanofibers was not significantly changed as ca. 90% with elevating temperature up to 300 °C. In addition, the CP/MAS ^{13}C NMR spectrum of the stretched cellulose nanofibrous

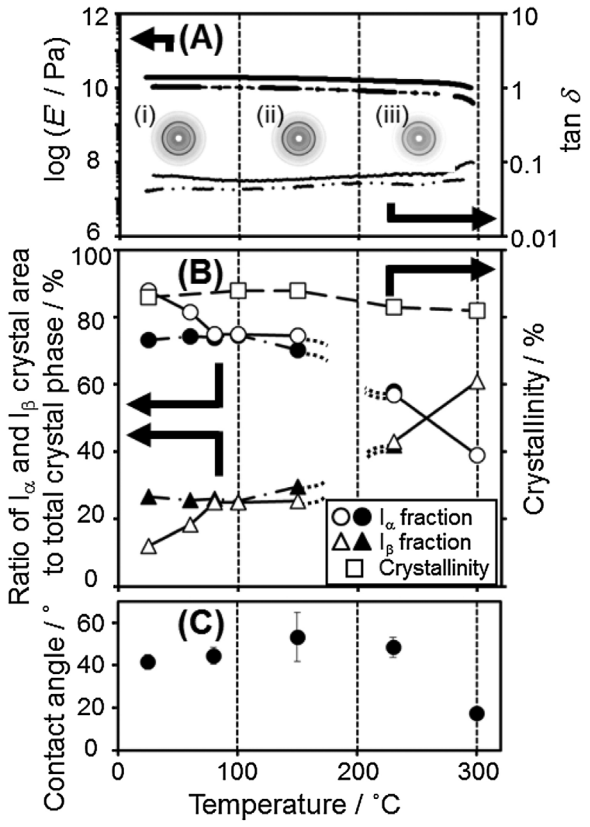

Fig. 5. (a) Temperature dependence of the dynamic viscoelastic properties (E' and $\tan\delta$) of an unstretched nanofibrous film (dashed line) in comparison to the stretched film (continuous line) together with WAXD images for the drawn films (i) before heating and after heating at (ii) 230 °C and (iii) 300 °C. (b) The corresponding crystalline transformation in the nanofibrous film from the I_α crystalline phase to the I_β crystalline phase with increasing temperature together with changes in the crystallinity and I_β crystalline phases of the cellulose pellicle produced in the culture medium covered with silicone oil (open circle, triangle and square) and non-covered (solid circle, and triangle). (c) The corresponding change in water contact angle on the surfaces of the stretched cellulose nanofibrous films.

film obtained after heating at 300 °C exhibited a line-broadening of the corresponding chemical shifts for the C-1, C-4 and C-6 carbons of the anhydroglucose unit (see Supporting Figure 1d), indicating that carbonization of the crystalline domains into graphite might have occurred, together with partial thermal degradation.

These behaviors may be attributed to a four-fold phenomenon: (i) the elevated temperature allowed the meta-stable I_α crystalline phase to transform into the cellulose I_β crystalline phase (Wada, Kondo, & Okano, 2003; Yamamoto & Horii, 1993). (ii) The transformation from the cellulose I_α crystalline phase to I_β occurred at the nanofiber surface. (iii) The cellulose I_α crystalline phase of the nanofibers cultured under the present condition, was less stable, resulting in crystalline transformation being more preferably induced under 80 °C, resulting in the nanofiber surface being covered with the more stable cellulose I_β crystalline phase. (iv) At 230 °C, thermal expansion (Wada, 2002) of the crystalline lattice including the inner crystalline domains might start to occur, encouraging the drastic transformation from the I_α crystalline phase to the I_β crystalline phase. Based on the above, it is considered that the microbial cellulose nanofibers produced by *G. xylinus* when cultured using dissolved oxygen in the culture medium are a new type of nanofiber that exhibits a different thermal response to those produced using normal bacterial cultures to date.

Considering the storage elastic moduli, E', values along the stretching direction depending upon the % crystalline fraction of the cellulose I_α crystalline phase with heating, together with the corresponding Young's moduli values (see Supporting Table), the E' values maintained almost the same value after heating as stated above. Meanwhile, the Young's modulus changed with heating temperature. Before heating, the Young's modulus of the nanofibrous film stretched up to 1.5 times was ca. 7.0 GPa, which is about three times greater than that of the non-stretched transparent nanofibrous film. This Young's modulus value is comparable to that of a conventional poly(ethylene terephthalate) film stretched up to 4 times (Kunugi, Ichinose, & Suzuki, 1986). Then, during heating to 230 °C, the Young's modulus of the stretched nanofibrous film increased to 12.0 GPa. The obtained results indicate that the increase in Young's modulus is strongly dependent on the % crystalline fraction of the I_α crystalline phase in the nanofibers. Finally, the Young's modulus decreased to ca. 4.7 GPa until 300 °C. The stretched nanofibrous film gradually darkened in color as the temperature changed from 230 °C to 300 °C. Thus, it was considered that carbonization of the stretched nanofibrous film occurred, to some extent, from around 230 °C onwards, as supported by the CP/MAS ^{13}C NMR results as stated previously. This stretched cellulose nanofibrous film is comparable to conventional high-performance synthetic polymeric materials having good mechanical properties (Brandrup & Immergut, 1989; Takayanagi, 1967) (see Supporting Figure 3a). However, such materials cannot often maintain such physical properties under high temperature (Supporting Figure 3b). Therefore, it should be emphasized that the well-oriented cellulose nanofibrous film prepared from the microbial gel-like material in this study, which is more than 90% rich in the cellulose I_α crystalline phase, exhibits a superior thermal stability to conventional high-performance synthetic polymeric materials.

Fig. 6c shows the observed change in contact angle on the surface of the stretched cellulose nanofibrous films, accompanied by the transformation of the I_α crystalline phase with elevating temperature. When the film was heated to less than 100 °C, the value of the contact angles was maintained at ca. 15°. However, the contact angle increased drastically when heated to 150 °C. This indicates that heating over 130 °C completely dried the film samples by removal of free and absorbed water (Tomita et al., 2009). At temperatures over 150 °C, the contact angle decreased slightly until 300 °C. In addition, the AFM observation of the film surface indicated that there was no significant contribution of surface roughness (RMS: 40 nm) to the change in contact angle. Therefore, the change in the contact angle was likely due to the crystalline transformation from the cellulose I_α crystalline phase to the I_β crystalline phase on the nanofiber surface. Namely, the film surface consisting of fibers adopting the cellulose I_β crystalline phase is more hydrophobic than the film surface consisting of fibers adopting the I_α crystalline phase.

Dependence of physical properties of stretched films on relative humidity. To examine the influence of water vapor on the physical properties of the cellulose nanofibrous films described above, the corresponding measurements were also performed under desired relative humidity. Prior to the influence of water vapor, the mechanical strength of the nanofibrous film was found to be fairly weak (see Fig. 7d) when compared with that for the normal pellicle produced by *G. xylinus*. This could be due to the lower population density of the thinner nanofibers in the present sample as compared with the normal sample, which also contributes to a reduced likelihood of the nanofibers engaging in the formation of crosslinkages in the nanofibrous film. This relationship, including the biosynthesis of nanocellulose from the bacterium under this oxygen-lacking environment, should require more detailed investigation.

Fig. 6 shows the changes in values of the storage elastic modulus, E', contact angle, Young's modulus, and tensile strength, as well as the elongation at break value, of the nanofibrous films according to

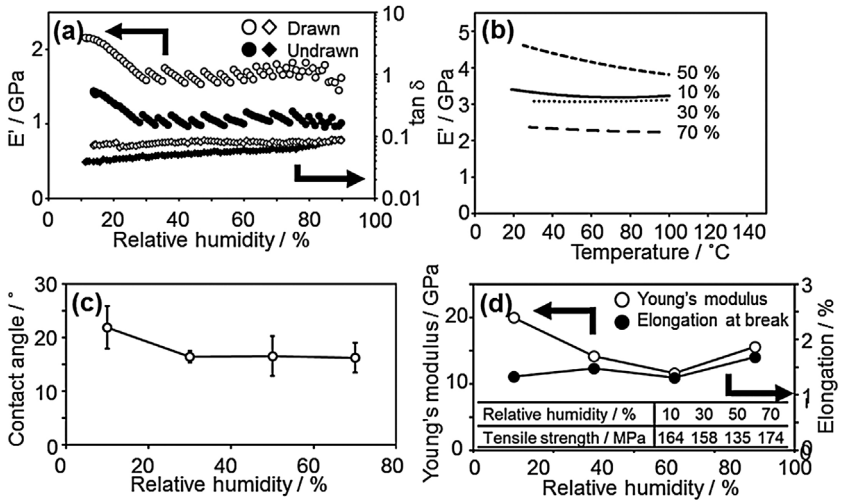

Fig. 6. Dependence of the stretched film properties on relative humidity. (a) Dynamic viscoelastic properties (E': circles and tan δ: diamonds) of an undrawn film (solid) in comparison to the drawn film (open), (b) temperature dependence of E' of (a), (c) with respect to a change in the contact angle, and (d) mechanical properties.

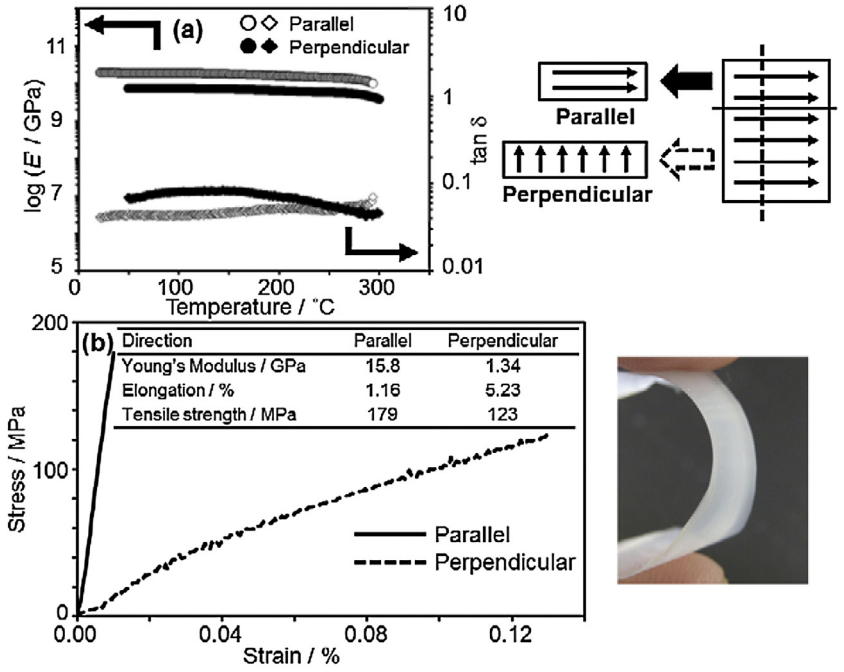

Fig. 7. Anisotropic viscoelastic and mechanical properties of the obtained oriented nanofibrous film: Parallel and perpendicular direction to the stretching direction. (a) Temperature dependence of the dynamic viscoelastic properties (E': circles and tan δ: diamonds), and (b) the anisotropy of the mechanical properties together with physical values. The photo shows the apparent flexibility of the oriented nanofibrous film bent with fingers.

the relative humidity in the atmosphere. According to the contact angle measurements in Fig. 6c, the film surface may become somehow wet, thereby resulting in a slight decrease of the angle under less than 30% humidity, before becoming saturated. This wettability affected the E' value, and Young's modulus possibly from 10 to 30% of the relative humidity as seen in Fig. 6a, c, and d. The stretched cellulose microbial nanofibrous film did not exhibit a drastic change in any of the range of measurements made from 10 to 90% humidity, except for the case at 50% humidity. We have not yet found a reasonable explanation for the particular 50% case, but one possibility is due to the heterogeneity in the film thickness that could make the properties deviate greatly. Considering the above, after the cellulose nanofibrous film was completely dried at 130 °C, the oriented nanofibrous film is no longer influenced by ambient water vapor.

3.4. Anisotropic properties of stretched nanofibrous films as a template for 3D-fabrication using biological systems

As stated previously, the microbial cellulose nanofibers in the stretched nanofibrous film are apparently well oriented. Therefore, anisotropy in the viscoelastic and mechanical properties was examined at directions both parallel and perpendicular (see the inserted sketch in Fig. 7) to the stretching direction. The E' value (Fig. 7a) and Young's modulus (Fig. 7b) were higher in the parallel direction than in the perpendicular direction, by more than one hundred times and ten times, respectively. It is noted that the degree of difference in the elongation at break value for the perpendicular direction was much greater than that for the tensile strength value. These results indicated that the obtained nanofibrous film was fairly flexible, although it showed anisotropic effects (see the photo in Fig. 7).

In relation to our previous studies (Higashi & Kondo, 2012; Kondo & Kasai, 2014; Kondo et al., 2002, 2012; Seyama, Suh, & Kondo, 2013) on nematic ordered cellulose (NOC) as a template for 3D-fabrication using biological systems, the obtained oriented nanofibrous film was examined as a template for epitaxial deposition of nanofibers secreted by *G. xylinus*. When active *G. xylinus* cells were transferred to the oriented surface, they started to synthesize cellulose ribbons that parallel the nanofiber orientation of the substrate. This was evidenced by direct video imaging of the motion of the bacterium as it synthesized the cellulose ribbon. The cell movement (at a constant rate of 3.2 $\mu m\,min^{-1}$ at 24 °C) was the result of an inverse force imposed by the directed polymerization and crystallization of the cellulose along the orientation direction as the track of the nanofibers. The rate of 3.2 $\mu m\,min^{-1}$ was faster than 2.4 $\mu m\,min^{-1}$ on the non-stretched film, but slower than 4.5 $\mu m\,min^{-1}$ for nematic ordered cellulose (NOC) templates (Kondo et al., 2002) at the same surrounding temperature. This bio-directed epitaxial nano-deposition could be studied over time.

It is noted that the bacterium moving along the nanofiber tracks rotated the head, but the tail appeared to be attached the tracks to continue the moving (see Supporting Figure 4). The results indicated that the secreted nanofiber from the bacterium was selectively attached to the oriented nanofiber on the stretched template to induce the controlled direction of the movement (Kondo et al., 2002, 2012). Namely, *G. xylinus* results in moving with secretion of a cellulose nanofiber along the nanofibrous track on the stretched film. Accordingly, the obtained oriented nanofibrous film can be expected as a template or scaffolds for 3D-fabrication using biological systems, similar to NOC film template as previously reported (Higashi & Kondo, 2012; Kondo & Kasai, 2014; Kondo et al., 2002, 2012; Seyama et al., 2013).

4. Conclusion

A new type of cellulose nanofiber pellicle was produced by *G. xylinus* using oxygen dissolved in the culture medium, instead of gaseous oxygen drawn from the atmosphere. The highly crystallized cellulose nanofibers, which were up to two thirds thinner than the cellulose nanofibers secreted by *G. xylinus* cultured in normal SH culture medium, were found to be dominantly composed of (ca. 90% fraction) the cellulose I_α crystalline phase. Moreover, the resulting cellulose pellicle could be stretched by up to 1.5 times due to the lower crosslinking density of cellulose nanofibers, resulting in a uniaxially well-oriented nanofibrous film. This film exhibited various unique characteristics including good thermal stability and anisotropy in both its viscoelastic and mechanical properties, which are related to the surface wettability, and presumably accompanied by a preferable thermal transformation of the crystalline form from the rich cellulose I_α crystalline phase to the I_β crystalline phase.

In the present study, we also want to emphasize that as a low-energy process, the microbial fabrication under an oxygen-lacking, stressed environment could offer a promising nanofibrous film rich in the cellulose I_α crystalline phase, which opens up the potential of this nanofibrous film for application as a scaffold, reinforcement material, or other structural material.

Acknowledgements

The authors thank Mr. Eiji Togawa of the Forestry and Forest Products Research Institute (FFPRI) for conducting the WAXD and CP/MAS ^{13}C NMR measurements. The authors also are indebted to Mr. Ryunosuke Funahashi of an undergraduate student at Kyushu University for his helpful contribution to the experiments. This study is partly supported by Grants-in-Aid for Scientific Research (Nos. 22380097 & 23658146) from the Japan Society for the Promotion of Science.

Appendix A. Supplementary data

Supplementary data associated with this article can be found, in the online version, at doi:10.1016/j.carbpol.2015.08.077.

References

Atalla, R. H., & VanderHart, D. L. (1984). Native cellulose. A composite of two distinct crystalline forms. *Science*, *223*, 283–285.
Bäckdahl, H., Esguerra, M., Delbro, D., Risberg, B., & Gatenholm, P. (2008). Engineering microporosity in bacterial cellulose scaffolds. *Journal of Tissue Engineering and Regenerative Medicine*, *2*, 320–330.
Bae, S., & Shoda, M. (2005). Statistical optimization of culture conditions for bacterial cellulose production using Box-Behnken design. *Biotechnology and Bioengineering*, *90*, 20–28.
Benziman, M., & Rivetz, B. (1972). Factors affecting hexose phosphorylation in *Acetobacter xylinum*. *Journal of Bacteriology*, *111*, 325–333.
Blaker, J. J., Lee, K.-Y., Li, X., Menner, A., & Bismarck, A. (2009). Renewable nanocomposite polymer foams synthesized from Pickering emulsion templates. *Green Chemistry*, *11*, 1321–1326.
Bodin, A., Concaro, S., Brittberg, M., & Gatenholm, P. (2007). Bacterial cellulose as a potential meniscus implant. *Journal of Tissue Engineering and Regenerative Medicine*, *1*, 406–408.
Bohn, A., Fink, H.-P., Ganster, J., & Pinnow, M. (2000). X-ray texture investigations of bacterial cellulose. *Macromolecular Chemistry and Physics*, *201*, 1913–1921.
Brandrup, J., & Immergut, E. H. (1989). *Polymer handbook* (3rd ed., pp. 23). NY, USA: John Wiley & Sons, Inc. Section V
Chao, Y., Sugano, Y., & Shoda, M. (2001). Bacterial cellulose production under oxygen-enriched air at different fructose concentrations in a 50-liter, internal-loop airlift reactor. *Applied Microbiology and Biotechnology*, *55*, 673–679.
Cheng, H.-P., Wang, P.-M., Chen, J.-W., & Wu, W.-T. (2002). Cultivation of *Acetobacter xylinum* for bacterial cellulose production in a modified airlift reactor. *Biotechnology and Applied Biochemistry*, *35*, 125–132.
Helenius, G., Bäckdahl, H., Bodin, A., Nannmark, U., Gatenholm, P., & Risberg, B. (2006). *In vivo* biocompatibility of bacterial cellulose. *Journal of Biomedical Materials Research Part A*, *76A*, 431–438.
Hestrin, S., & Schramm, M. (1954). Synthesis of cellulose by *Acetobacter xylinum*. II. Preparation of freeze-dried cells capable of polymerizing glucose to cellulose. *Biochemical Journal*, *58*, 345–352.
Higashi, K., & Kondo, T. (2012). Nematic ordered cellulose templates mediating order-patterned deposition accompanied with synthesis of calcium phosphates. *Cellulose*, *19*, 81–90.
Hishikawa, Y., Togawa, E., & Kondo, T. (2010). Molecular orientation in the nematic ordered cellulose film using polarized FTIR accompanied with a vapor-phase deuteration method. *Cellulose*, *17*, 539–545.
Horii, F., Yamamoto, H., Kitamaru, R., Tanahashi, M., & Higuchi, T. (1987). Transformation of native cellulose crystals induced by saturated steam at high temperatures. *Macromolecules*, *20*, 2946–2949.
Hwang, J. W., Yang, Y. K., Hwang, J. K., Pyun, Y. R., & Kim, Y. S. (1999). Effects of pH and dissolved oxygen on cellulose production by *Acetobacter xylinum* BRC5 in agitated culture. *Journal of Bioscience and Bioengineering*, *88*, 183–188.
Kataoka, Y., & Kondo, T. (1996). Changing cellulose crystalline structure in forming wood cell walls. *Macromolecules*, *29*, 6356–6358.
Kataoka, Y., & Kondo, T. (1998). FT-IR microscopic analysis of changing cellulose crystalline structure during wood cell wall formation. *Macromolecules*, *31*, 760–764.
Kataoka, Y., & Kondo, T. (1999). Quantitative analysis for the cellulose I_α crystalline phase in developing wood cell walls. *International Journal of Biological Macromolecules*, *24*, 37–41.
Kimura, S., Chen, H. P., Saxena, I. M., Brown, R. M., Jr., & Itoh, T. (2001). Localization of c-di-GMP-binding protein with the linear terminal complexes of *Acetobacter xylinum*. *Journal of Bacteriology*, *183*, 5668–5674.
Kondo, T. (1997). The assignment of IR absorption bands due to free hydroxyl groups in cellulose. *Cellulose*, *4*, 281–292.
Kondo, T., Nojiri, M., Hishikawa, Y., Togawa, E., Romanovicz, D., & Brown, R. M., Jr. (2002). Biodirected epitaxial nanodeposition of polymers on oriented macromolecular templates. *Proceedings of the National Academy of Sciences of the United States of America*, *99*, 14008–14013.
Kondo, T., Kasai, W., Nojiri, M., Hishikawa, Y., Togawa, E., Romanovicz, D., et al. (2012). Regulated patterns of bacterial movements based on their secreted cellulose nanofibers interacting interfacially with ordered chitin templates. *Journal of Bioscience and Bioengineering*, *114*, 113–120.
Kondo, T., & Kasai, W. (2014). Autonomous bottom-up fabrication of three-dimensional nano/microcellulose honeycomb structures, directed by bacterial nanobuilder. *Journal of Bioscience and Bioengineering*, *118*, 482–487.
Kose, R., Kasai, W., & Kondo, T. (2011). Switching surface properties of substrates by coating with a cellulose nanofiber having a high adsorbability. *Sen'i Gakkaishi*, *67*, 163–168 (in Japanese).

Kose, R., Mitani, I., Kasai, W., & Kondo, T. (2011). "Nanocellulose" as a Single nanofiber prepared from pellicle secreted by *Gluconacetobacter xylinus* using aqueous counter collision. *Biomacromolecules*, *12*, 716–720.
Kose, R., & Kondo, T. (2013). Size effects of cellulose nanofibers for enhancing the crystallization of poly(lactic acid). *Journal of Applied Polymer Science*, *128*, 1200–1205.
Kunugi, T., Ichinose, C., & Suzuki, A. (1986). Preparation of high-modulus and high-strength poly(ethylene terephthalate) film by zone-annealing method. *Journal of Applied Polymer Science*, *31*, 429–439.
Marrinan, H. J., & Mann, J. (1956). Infrared spectra of the crystalline modifications of cellulose. *Journal of Polymer Science*, *XXI*, 301–311.
Naritomi, T., Kouda, T., Yano, H., Yoshinaga, F., Shigematsu, T., Morimura, S., et al. (2002). Influence of broth exchange ratio on bacterial cellulose production by repeated-batch culture. *Process Biochemistry*, *38*, 41–47.
Nielsen, L. E., & Landel, R. F. (1994). *Mechanical properties of polymers and composites* (2nd ed., pp. 268–277). NY, USA: Marcel Dekker, Inc. Chapter 5.
Ross, P., Mayer, R., & Benziman, M. (1991). Cellulose biosynthesis and function in bacteria. *Microbiological Reviews*, *55*, 35–58.
Setyawati, M. I., Chien, L.-J., & Lee, C.-K. (2007). Expressing *Vitreoscilla* hemoglobin in statically cultured *Acetobacter xylinum* with reduced O_2 tension maximizes bacterial cellulose pellicle production. *Journal of Biotechnology*, *132*, 38–43.
Seyama, T., Suh, E.-Y., & Kondo, T. (2013). Three-dimensional culture of epidermal cells on ordered cellulose scaffolds. *Biofabrication*, *5*, 025010 (5pp).
Shah, J., & Brown, R. M., Jr. (2005). Towards electronic paper displays made from microbial cellulose. *Applied Microbiology and Biotechnology*, *66*, 352–355.
Sugiyama, J., Okano, T., Yamamoto, H., & Horii, F. (1990). Transformation of *Valonia* cellulose crystals by an alkaline hydrothermal treatment. *Macromolecules*, *23*, 3196–3198.
Sugiyama, J., Persson, J., & Chanzy, H. (1991). Combined infrared and electron diffraction study of the polymorphism of native celluloses. *Macromolecules*, *24*, 2461–2466.
Swissa, M., Aloni, Y., Weinhouse, H., & Benizman, M. (1980). Intermediary steps in *Acetobacter xylinum* cellulose synthesis. Studies with whole cells and cell-free preparations of the wild type and a celluloseless mutant. *Journal of Bacteriology*, *143*, 1142–1150.
Takayanagi, M. (1967). Crystallized state of polymer in its dispersion behavior. *Pure and Applied Chemistry*, *15*, 555–586.
Togawa, E., & Kondo, T. (1999). Change of morphological properties in drawing water-swollen cellulose films prepared from organic solutions. A view of molecular orientation in the drawing process. *Journal of Polymer Science Part B: Polymer Physics*, *37*, 451–459.
Tomita, Y., Tsuji, T., & Kondo, T. (2009). Fabrication of microbial cellulose nanofiber network sheets hydrophobically enhanced by introduction of a heat-printed surface. *Sen'i Gakkaishi*, *65*, 73–79 (in Japanese).
Vandamme, E. J., Baets, S. D., Vandaelen, A., Joris, K., & Wulf, P. D. (1998). Improved production of bacterial cellulose and its application potential. *Polymer Degradation and Stability*, *59*, 93–99.
VanderHart, D. L., & Atalla, R. H. (1984). Studies of microstructure in native celluloses using solid-state ^{13}C NMR. *Macromolecules*, *17*, 1465–1472.
Wada, M. (2002). Lateral thermal expansion of cellulose I_β and III_I polymorphs. *Journal of Polymer Science Part B: Polymer Physics*, *40*, 1095–1102.
Wada, M., Kondo, T., & Okano, T. (2003). Thermally induced crystal transformation from cellulose I_α to I_β. *Polymer Journal*, *35*, 155–159.
Watanabe, K., & Yamanaka, S. (1995). Effects of oxygen tension in the gaseous phase on production and physical properties of bacterial cellulose formed under static culture conditions. *Bioscience, Biotechnology, and Biochemistry*, *59*, 65–68.
Yamamoto, H., & Horii, F. (1993). CP/MAS ^{13}C NMR analysis of the crystal transformation induced for *Valonia* cellulose by annealing at high temperatures. *Macromolecules*, *26*, 1313–1317.
Yamamoto, H., & Horii, F. (1994). *In situ* crystallization of bacterial cellulose I. Influences of polymeric additives, stirring and temperature on the formation celluloses I_α and I_β as revealed by cross polarization/magic angle spinning (CP/MAS) ^{13}C NMR spectroscopy. *Cellulose*, *1*, 57–66.
Yamamoto, H., Horii, F., & Hirai, A. (1996). *In situ* crystallization of bacterial cellulose. II. Influences of different polymeric additives on the formation of celluloses I_α and I_β at the early stage of incubation. *Cellulose*, *3*, 229–242.
Yamanaka, S., Watanabe, K., & Kitamura, N. (1989). The structure and mechanical properties of sheets prepared from bacterial cellulose. *Journal of Materials Science*, *24*, 3141–3145.
Yano, H., Sugiyama, J., Nakagaito, A. N., Nogi, M., Matsuura, T., Hikita, M., et al. (2005). Optically transparent composites reinforced with networks of bacterial nanofibers. *Advanced Materials*, *17*, 153–155.
Zbinden, R. (1964). *Infrared spectroscopy of high polymers*. New York: Academic Press.